

MATHEMATICAL MODELING OF ELECTROMAGNETIC FIELD PROFILES IN THE MICROWAVE OVEN

Apostolos Kokkosis

Department of Electronics, T.E.I of Piraeus

Abstract : The Mathematical modeling is widely used for representing transport phenomena using numerical equations. The solutions for these equations, when solved properly, would be in close agreement with the behaviour of the material. In microwave heating, modelling can be a design tool to understand and develop optimum heating procedure for food. In the modelling process, the food system is broken down into many small elements. Simulation of the source of microwave is possible and solution to the electric field equations can be obtained. In the present study, a mathematical modelling technique, based on the finite element method was employed to analyze the heating behaviour.

Περίληψη: Η μαθηματική μοντελοποίηση χρησιμοποιείται ευρύτατα στην απεικόνιση φαινομένων μεταφοράς με τη χρήση αριθμητικών εξισώσεων. Η σωστή επίλυση αυτών των εξισώσεων, είναι σύμφωνη με τη συμπεριφορά των υλικών. Στη μικροκυματική θέρμανση, η μοντελοποίηση μπορεί να γίνει ένα εργαλείο σχεδίασης για την κατανόηση και την ανάπτυξη βέλτιστων διαδικασιών θέρμανσης των τροφίμων. Στη διαδικασία μοντελοποίησης, το σύστημα των τροφίμων διασπάται σε πολλά μικρά στοιχεία. Είναι δυνατόν να πραγματοποιηθεί η προσομοίωση της πηγής των μικροκυμάτων και έτσι μπορεί να αποκτηθεί μια λύση στις εξισώσεις του ηλεκτρικού πεδίου. Στην παρούσα μελέτη, αναπτύσσεται μια τεχνική μαθηματικής μοντελοποίησης, που βασίζεται στη μέθοδο πεπερασμένων στοιχείων για την ανάλυση της συμπεριφοράς θέρμανσης..

1. Introduction

The system for generating and utilizing the microwaves at 2,45 GHz is presented in Fig.1. The geometrical dimensions of the oven, offers us the possibility to heat medium size bodies, till 40 cm long. In Fig.2, can be seen the microwave oven with the sample.

The study of the electromagnetic field in a microwave oven and the following of the distribution and the values of the field, gives us some very important information about the heating process itself.

The waveguide structures in Fig 3a and 3b also used in the microwave oven, do not support the TEM mode (Transversal Electromagnetic Mode). They do support higher-order modes or field structures where the magnetic field is transverse to the line axis-the TM or transverse magnetic mode, $H_z=0$ or the electric field is transverse to the line axis-the TE or transverse electric mode, $E_z=0$.

The cavity is excited by one magnetron (frequency 2.45 GHz, average power 1 kW) through the waveguide feeder where the dominant (TE_{10}) mode is generated; the walls are of perfect electric conductivity. A waveguide can be designed to support only the TE_{10} mode by selecting the guide dimensions such that the operating frequency (2,45 GHz) is greater than cutoff frequency for the mode TM_{11} and it's less than the cutoff frequency of the higher mode.

The cutoff frequency of the TM_{mn} mode is:

$$f_{c,mn} = \frac{1}{2\pi\sqrt{\mu\epsilon}} \sqrt{\left(\frac{m\pi}{a}\right)^2 + \left(\frac{n\pi}{b}\right)^2}$$

$$\text{we have: } \begin{cases} a = 7 \cdot 10^{-2} m \\ b = 13,5 \cdot 10^{-2} m \end{cases}$$

The cutoff frequency for our dimensions of the microwave oven waveguide feeder is:

$$f_{c,11} = 1,5 \cdot 10^8 \sqrt{\left(\frac{1}{7 \cdot 10^{-2}}\right)^2 + \left(\frac{1}{13,5 \cdot 10^{-2}}\right)^2} = 1,5 \cdot 10^8 \sqrt{204 + 54} = 1,5 \cdot 10^8 \cdot 16 = 2,4GHz$$

$$f_{c,12} = 1,5 \cdot 10^8 \sqrt{\left(\frac{1}{7 \cdot 10^{-2}}\right)^2 + \left(\frac{2}{13,5 \cdot 10^{-2}}\right)^2} = 1,5 \cdot 10^8 \sqrt{204 + 4 \cdot 54} = 1,5 \cdot 10^8 \cdot 20,49 = 3,07GHz$$

$$f_{c,11} = 1,5 \cdot 10^8 \sqrt{\left(\frac{2}{7 \cdot 10^{-2}}\right)^2 + \left(\frac{1}{13,5 \cdot 10^{-2}}\right)^2} = 1,5 \cdot 10^8 \sqrt{4 \cdot 204 + 54} = 1,5 \cdot 10^8 \cdot 29,49 = 4,42GHz$$

$f_{c,11} < f_{c,12} < f_{c,21} \Rightarrow TE$ mode for the waveguide feeder

$$f_{c,10} = \frac{1}{2\pi\sqrt{\mu\epsilon}} \frac{\pi}{a} = \frac{1}{2a\sqrt{\mu\epsilon}} = \frac{u}{2a}$$

$$f_{c,10} = 1,5 \cdot 10^8 \cdot 7 \cdot 10^{-2} = 2,14GHz$$

The possibility of simultaneous existence of both forward and backward travelling waves suggests the possibility of standing waves and resonant behaviour. Suppose we insert conducting plates at $z=0$ and $z=d$, as shown in Fig. 4. These conducting plates give rise to reflections at the waveguide fields, resulting in standing waves. In this section we will investigate the resulting fields and the resonant frequencies of this cavity.

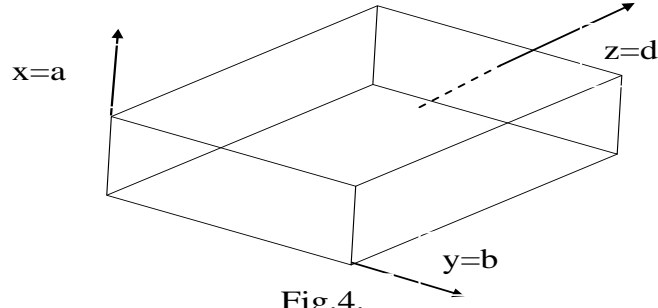


Fig.4.

3. TM modes

The total field in these sum of these forward- and backward-traveling waves are:

$$\hat{E}_z = \hat{E}_z^+ + \hat{E}_z^- = \sin \beta_x x \sin \beta_y y (C^+ e^{-\gamma z} + C^- e^{-\gamma z}) \quad (1)$$

Substituting these field individually into the solutions for other field components of the wave equation of the guide and remembering that γ is to be replaced with $-\gamma$ in these equations for the backward-traveling waves yields, from the results for the TM modes for rectangular waveguides we obtain:

$$\left\{ \begin{array}{l} \hat{E}_x = \frac{\beta_x}{\beta_x^2 + \beta_y^2} \cos \beta_x x \sin \beta_y y (-\gamma C^+ e^{-\gamma z} + \gamma C^- e^{\gamma z}) \\ \hat{E}_y = \frac{\beta_y}{\beta_x^2 + \beta_y^2} \sin \beta_x x \cos \beta_y y (-\gamma C^+ e^{-\gamma z} + \gamma C^- e^{\gamma z}) \\ \hat{H}_x = \frac{j\omega\epsilon\beta_y}{\beta_x^2 + \beta_y^2} \sin \beta_x x \cos \beta_y y (C^+ e^{-\gamma z} + C^- e^{\gamma z}) \\ \hat{H}_y = \frac{-j\omega\epsilon\beta_x}{\beta_x^2 + \beta_y^2} \cos \beta_x x \sin \beta_y y (C^+ e^{-\gamma z} + C^- e^{\gamma z}) \end{array} \right. \quad (2)$$

where:

$$\beta_x = \frac{m\pi}{a} \quad (3)$$

$$\beta_y = \frac{n\pi}{b}$$

The boundary conditions imposed by the plates at $z=0$ and $z=d$ require:

$$\left\{ \begin{array}{l} \hat{E}_y = 0 \\ \hat{E}_x = 0 \end{array} \right. \quad \text{at } z=0, z=d \quad (4)$$

From (2) we see that this requires:

$$-\hat{C}^+ e^{-\gamma z} + \hat{C}^- e^{\gamma z} = 0$$

at $z=0$ and $z=d$. Thus, $\hat{C}^+ = \hat{C}^- = \hat{C}$ and $\lambda = j\frac{p\pi}{d} \triangleq j\beta_z$ (5)

where $p=1,2,\dots$, and we define:

$$\beta_z = \frac{p\pi}{d} \quad (6)$$

Substituting (5) into (2) gives:

$$\begin{cases} \hat{E}_x = -\frac{2\beta_x\beta_z\hat{C}}{\beta_x^2 + \beta_y^2} \cos\beta_x x \sin\beta_y y \sin\beta_z z \\ \hat{E}_y = -\frac{2\beta_y\beta_z\hat{C}}{\beta_x^2 + \beta_y^2} \sin\beta_x x \cos\beta_y y \sin\beta_z z \end{cases}$$

Using these results in (2) yields:

$$\begin{cases} \hat{E}_z = 2\hat{C} \sin\beta_x x \sin\beta_y y \cos\beta_z z \\ \hat{H}_x = \frac{2j\omega\varepsilon\beta_y\hat{C}}{\beta_x^2 + \beta_y^2} \sin\beta_x x \cos\beta_y y \cos\beta_z z \\ \hat{H}_y = -\frac{2j\omega\varepsilon\beta_x\hat{C}}{\beta_x^2 + \beta_y^2} \cos\beta_x x \sin\beta_y y \cos\beta_z z \end{cases}$$

The time-domain forms of the fields can easily be obtained by multiplying each phasor by $e^{j\omega t}$ and taking the real part of the result. Since these phasors do not contain isolated, complex exponentials, the time-domain fields will vary with time as $\sin(\omega t)$ or $\cos(\omega t)$. Thus the fields are oscillatory.

Each set of integers m , n , and p is said to be associated with a TM_{mnp} mode. The resonant frequency of each mode is calculated by substituting (5) into $(\gamma^2 + \omega^2 \mu\varepsilon) = \beta_x^2 + \beta_y^2$

$$f_{c,mnp} = \frac{1}{2\pi\sqrt{\mu\varepsilon}} \sqrt{\left(\frac{m\pi}{a}\right)^2 + \left(\frac{n\pi}{b}\right)^2 + \left(\frac{p\pi}{d}\right)^2} = \frac{u}{2} \sqrt{\left(\frac{m}{a}\right)^2 + \left(\frac{n}{b}\right)^2 + \left(\frac{p}{d}\right)^2} \quad (9)$$

Equations (8) show that neither m or n can be zero; otherwise, all field components vanish. However, p can be zero. Thus, the lowest-order TM mode is the TM_{110} mode.

4. TE modes

A similar development can be obtained for the TE modes. The total fields are:

$$\hat{H}_z = \hat{H}_z^+ + \hat{H}_z^- = \cos\beta_x x \cos\beta_y y (C^+ e^{-jyz} + C^- e^{-jyz}) \quad (10)$$

$$\left\{ \begin{aligned} \hat{H}_x &= \frac{\beta_x}{\beta_x^2 + \beta_y^2} \sin \beta_x x \cos \beta_y y (\gamma C^+ e^{-\gamma z} - \gamma C^- e^{\gamma z}) \\ \hat{H}_y &= \frac{\beta_y}{\beta_x^2 + \beta_y^2} \cos \beta_x x \sin \beta_y y (\gamma C^+ e^{-\gamma z} - \gamma C^- e^{\gamma z}) \\ \hat{E}_x &= \frac{j\omega\varepsilon\beta_y}{\beta_x^2 + \beta_y^2} \cos \beta_x x \sin \beta_y y (C^+ e^{-\gamma z} + C^- e^{\gamma z}) \\ \hat{E}_y &= \frac{-j\omega\varepsilon\beta_x}{\beta_x^2 + \beta_y^2} \sin \beta_x x \cos \beta_y y (C^+ e^{-\gamma z} + C^- e^{\gamma z}) \end{aligned} \right. \quad (11)$$

The boundary conditions imposed by the conductors at $z=0$ and $z=d$ are given by (4), once again yielding (5) and (6). Substituting it to (11) yields:

$$\left\{ \begin{aligned} \hat{H}_z &= j2\hat{C} \cos \beta_x x \cos \beta_y y \sin \beta_z z \\ \hat{H}_x &= -j \frac{2\beta_x \beta_z}{\beta_x^2 + \beta_y^2} \hat{C} \sin \beta_x x \cos \beta_y y \cos \beta_z z \\ \hat{H}_y &= -j \frac{2\beta_y \beta_z}{\beta_x^2 + \beta_y^2} \hat{C} \cos \beta_x x \sin \beta_y y \cos \beta_z z \\ \hat{E}_x &= -\frac{2\omega\mu\beta_y}{\beta_x^2 + \beta_y^2} \hat{C} \cos \beta_x x \sin \beta_y y \sin \beta_z z \\ \hat{E}_y &= \frac{\omega\mu\beta_x}{\beta_x^2 + \beta_y^2} \hat{C} \sin \beta_x x \cos \beta_y y \sin \beta_z z \end{aligned} \right. \quad (12)$$

The resonant frequency is the same as in the TM modes. Equations (12) show that either m or n (but not both) can be zero and that p cannot be zero. Hence, two lowest-order modes are the TE_{011} and TE_{101} modes.

The fields of the TE_{101} mode have the lowest resonant frequency if we assume $a \geq d \geq b$. For the TE_{101} mode the fields become:

$$\left\{ \begin{aligned} \hat{H}_z &= j2\hat{C} \cos \frac{\pi x}{a} \sin \frac{\pi z}{d} \\ \hat{H}_x &= -j2 \frac{a}{d} \hat{C} \sin \frac{\pi x}{a} \cos \frac{\pi z}{d} \\ \hat{E}_y &= \frac{2\omega\mu a}{\pi} \hat{C} \sin \frac{\pi x}{a} \sin \frac{\pi z}{d} \end{aligned} \right. \quad (13)$$

The electric field is y -directed and has a maximum at $x=a/2$ and $z=d/2$. Thus, in order to excite this mode efficiently, an electric field probe (say, coaxial cable with the center conductor exposed) could be inserted at the center of the side of largest area.

We will calculate the resonant frequency for the TM_{110} , TE_{101} and TE_{011} modes using the dimensions that are shown in Figure 2 in concordance with Figure 4.

$$\text{which are: } \begin{cases} a = 29 \cdot 10^{-2} m \\ b = 29 \cdot 10^{-2} m \\ d = 19 \cdot 10^{-2} m \end{cases}$$

We will use (9) and we must consider that a, b and c are in mm in Fig 2. so we have to transform them in meters to use in our equation and that u is the speed of light.

$$\begin{cases} f_{c,mnp} = \frac{u}{2} \sqrt{\left(\frac{m}{a}\right)^2 + \left(\frac{n}{b}\right)^2 + \left(\frac{p}{d}\right)^2} \\ f_{c,110} = 1.5 \cdot 10^8 \sqrt{\left(\frac{1}{29 \cdot 10^{-2}}\right)^2 + \left(\frac{1}{29 \cdot 10^{-2}}\right)^2} \\ f_{c,110} = 1.5 \cdot 10^8 \sqrt{11,89 + 11,89} \\ f_{c,110} = 0.731 \text{GHz} \end{cases}$$

$$\begin{cases} f_{c,101} = 1.5 \cdot 10^8 \sqrt{\left(\frac{1}{29 \cdot 10^{-2}}\right)^2 + \left(\frac{1}{19 \cdot 10^{-2}}\right)^2} \\ f_{c,101} = 1.5 \cdot 10^8 \sqrt{11,89 + 5,26} \\ f_{c,101} = 0.621 \text{GHz} \end{cases}$$

$$\begin{cases} f_{c,011} = 1.5 \cdot 10^8 \sqrt{\left(\frac{1}{29 \cdot 10^{-2}}\right)^2 + \left(\frac{1}{19 \cdot 10^{-2}}\right)^2} \\ f_{c,011} = 1.5 \cdot 10^8 \sqrt{11,89 + 5,26} \\ f_{c,011} = 0.621 \text{GHz} \end{cases}$$

From the values we obtained we can conclusion that the lowest frequency we can obtain for our microwave oven is more than 0,815GHz. Next we try to find a relation between m, n and p for our dimensions we chose in fig 2. and for the 2,45GHz resonant frequency.

$$\begin{cases} f_{c,mnp} = \frac{u}{2} \sqrt{\left(\frac{m}{a}\right)^2 + \left(\frac{n}{b}\right)^2 + \left(\frac{p}{d}\right)^2} \\ f_{c,110} = 1.5 \cdot 10^8 \sqrt{\left(\frac{m}{18,8 \cdot 10^{-2}}\right)^2 + \left(\frac{n}{25,1 \cdot 10^{-2}}\right)^2 + \left(\frac{p}{27 \cdot 10^{-2}}\right)^2} \\ f_{c,110} = 1.5 \cdot 10^8 \sqrt{28,29 \cdot m^2 + 15,87 \cdot n^2 + 13,71 \cdot p^2} \\ 16,3 = \sqrt{28,29 \cdot m^2 + 15,87 \cdot n^2 + 13,71 \cdot p^2} \end{cases}$$

where $m, n, p = 1, 2, 3, 4, \dots$

5. Standing waves in microwave ovens

The solution of the three-dimensional wave equation with boundary conditions (see e.g. [1]) gives standing waves in the three dimensions x , y and z , which altogether obey the equation:

$$\frac{1}{\lambda^2} = \frac{1}{\lambda_x^2} + \frac{1}{\lambda_y^2} + \frac{1}{\lambda_z^2} \quad (14)$$

The wavelengths λ_x , λ_y and λ_z are determined by the linear dimensions L_x , L_y and L_z of the chamber:

$$L_x = l \frac{\lambda_x}{2} \quad L_y = m \frac{\lambda_y}{2} \quad L_z = n \frac{\lambda_z}{2} \quad (15)$$

where l, m, n are natural numbers. The solutions for given (l, m, n) are denoted as modes of the resonator. Obviously equation (2) allows more than one possibility to satisfy the same given value of λ . In commercial microwave ovens, the dimensions L_x , L_y and L_z scatter

Table 1. All modes of a microwave oven of dimensions 29 cm \times 29 cm \times 19 cm, which lead to a wavelength in the interval 12.0 cm $< \lambda_0 <$ 12.5 cm. Four modes are quite close to the magnetron wavelength of 12.25 cm.

λ_0 (cm)	l	m	n
12.103	1	1	3
12.274	2	4	1
12.274	4	2	1
12.277	2	3	2
12.277	3	2	2
12.375	0	1	3

appreciably; e.g., a survey of about 20 different ovens gave values of $L_x = 28$ – 35 cm, $L_y = 27$ – 33 cm and $L_z = 17$ – 21 cm. In the following an example with $L_x = 29$ cm, $L_y = 29$ cm and $L_z = 19$ cm will be discussed. Equations (14) and (15) allow a number of resonator frequencies which lie close to the emitted magnetron frequency. Table 1 demonstrates that there are six possible

solutions in the wavelength range between 12 cm and 12.5 cm.

6. Quality factor

The quality factor Q [1, 7] is a measure of the energy losses and, hence, also the frequency width $\Delta\omega$ of the modes. Q gives the ratio of the energy stored in the resonator and the energy loss per cycle:

$$Q = \omega E / (dE/dt). \quad (16)$$

For $Q \gg 1$ this may be written as:

$$Q \approx \omega / \Delta\omega. \quad (17)$$

The energy losses are due to four factors. First, microwaves may exit through the housing of the microwave oven. Safety regulations ensure that this contribution is negligibly small. Second, losses occur due to absorption in the walls, third due to absorption in the food within in the cooking chamber (the desired mechanism), and fourth, there is the chance that microwaves are coupled back into the magnetron. The latter mechanism may play a role if the oven is used empty, and it should be avoided in order to ensure a long lifetime of the magnetron. The overall quality factor can be calculated from

$$1/Q = 1/Q_1 + 1/Q_2 + \dots \quad (18)$$

If the oven is used empty, wall losses are most important. They can be estimated from the penetration depth δ [1, 7]:

$$Q_{\text{empty}} \approx V/S\delta \quad (19)$$

where V is the volume and S the inner surface area of the chamber. Typically, with air-filled volumes of about $29 \times 29 \times 19 \text{ cm}^3$ and $\delta \approx 1 \text{ }\mu\text{m}$ one finds Q -values of the order of 10^4 . For frequencies of 2.45 GHz, this leads to frequency widths of only 0.25 MHz, i.e. the

3. How Q varies

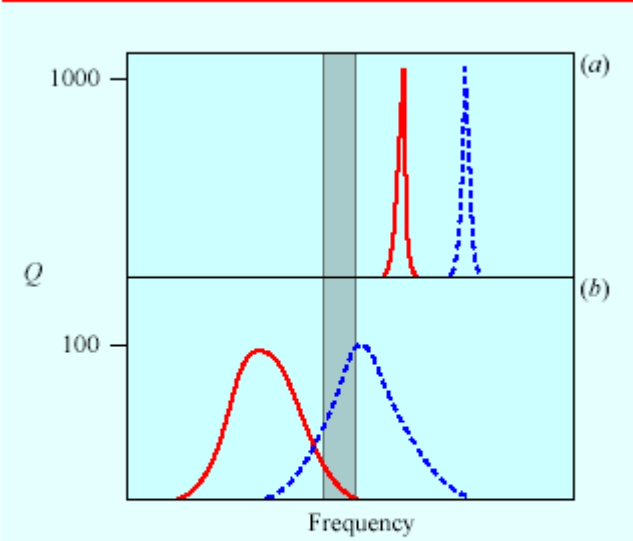


Figure 5. Schematic diagram showing how Q varies with frequency for two different modes of resonance in a microwave oven (not to scale): (a) with oven empty, (b) with food. The shaded band shows the frequency of the magnetron. If drawn to scale the widths of the modes in (b) would be about 100 times those in (a).

resonance modes are very narrow compared with the magnetron frequency width. Figure 5 depicts schematically a frequency spectrum of the modes of a cooking chamber. If some water containing food is placed in the chamber, i.e. a dielectric is inserted, the additional losses—being much larger than the wall losses—lead to a shift of the resonances to lower frequencies as well as an appreciable broadening of the modes. Due to the shifts and broadening, described by a quality factor that may well be of the order of 10^2 , more than one resonator mode may be excited. The larger the

oven and the more losses are present, the more modes may be excited simultaneously.

These multimode cavities have a more homogeneous field distribution, which is desirable for many applications, including cooking.

7. Quality factor

Food products release their moisture as steam during microwave cooking. When the food is cooked in a closed container, steam will accumulate in the headspace and this increases cooking efficiency. The model to be developed will take into account both the heat and mass (moisture) transfer during microwave cooking. To simplify the model following assumptions are considered.

- (1) The food product in the container was modeled as axisymmetric cylinder geometry (Figure 6).
- (2) Initial temperature and moisture distribution in the sample were assumed uniform.
- (3) Shrinkage of food product during microwave cooking was neglected.
- (4) Surface cooling is considered only due to evaporation and natural convection.
- (5) Bottom of the bowl receives negligible amount of energy due to reflection from the floor of the microwave oven during microwave heating.

Conduction heat transfer with heat generation within the food is the primary mode of heat transfer during microwave heating.

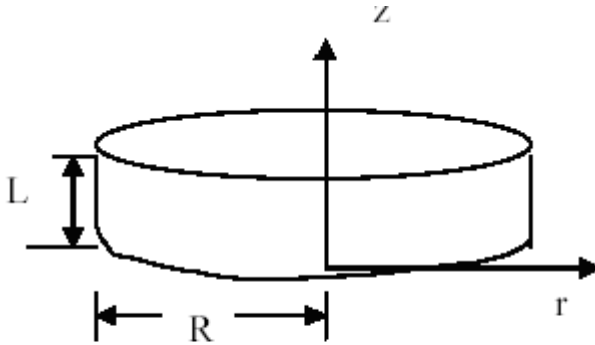


Fig. 6: Axisymmetric Model of the Food System

Axisymmetric transient heat transfer problem in cylindrical co-ordinates is governed by the partial differential equation:

$$K_{rr} \frac{\partial^2 T}{\partial r^2} + \frac{K_{rr}}{r} \frac{\partial T}{\partial r} + K_{zz} \frac{\partial^2 T}{\partial z^2} + Q = \rho C_p \frac{\partial T}{\partial t} \quad (20)$$

Assuming the thermal conductivity (k) as constant,

$$K \frac{\partial^2 T}{\partial r^2} + \frac{K}{r} \frac{\partial T}{\partial r} + K \frac{\partial^2 T}{\partial z^2} + Q = \rho C_p \frac{\partial T}{\partial t} \quad (21)$$

With initial condition: $T(r, z) = T_0$ at $t=0$ (22)

and the boundary conditions are:

$$-KA \frac{\partial T}{\partial r} = h_t A(T_s - T_a) + \lambda_v \frac{\partial m}{\partial t} \quad \text{at } r=R \quad (22)$$

$$-KA \frac{\partial T}{\partial z} = h_t A(T_s - T_a) + \lambda_v \frac{\partial m}{\partial t} \quad \text{at } z=L \quad (23)$$

The increase in temperature in the head space because of the steam release from the food during microwave heating can be calculated by heat balance:

$$V_h \rho_a C_{p_a} \frac{\partial T_a}{\partial t} = h_t A(T_s - T_a) \quad (24)$$

and mass transfer is given by,

$$\frac{\partial m}{\partial t} = h_m A(P_s - P_a) + \frac{\rho V C_p}{\lambda_v} \left(\frac{\partial T}{\partial t} \right) \quad (25)$$

Microwave energy entering the food from radial direction (r) and from longitudinal direction (z) must be considered in calculating the heat generation term (Q). Q is given by,

$$Q = Q_r \exp\left(\frac{-(R-r)}{\delta_p}\right) + Q_z \exp\left(\frac{-(L-z)}{\delta_p}\right) \quad (26)$$

The finite element method was used and the equations were solved over time by commercial software, FEMLAB.. Linear triangle elements were used and the number of elements was 1634 and the number of nodes was 878 (Figure 7).

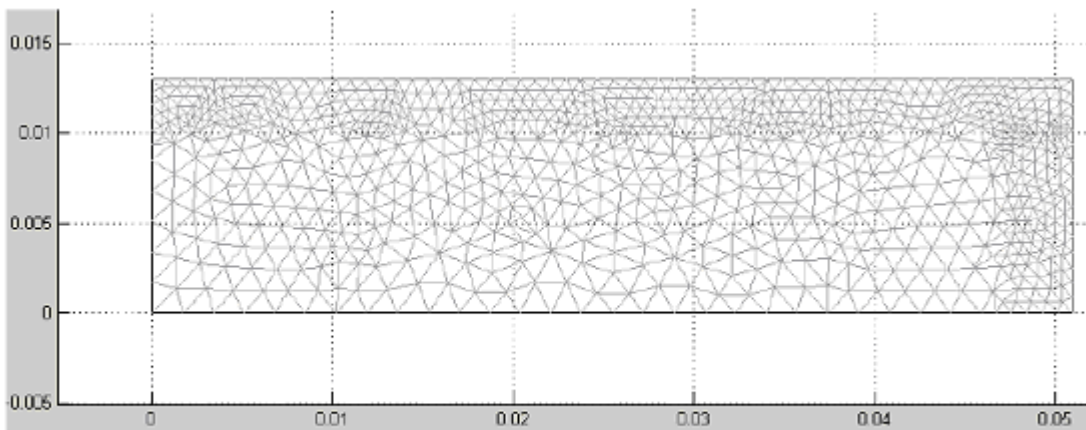


Fig. 7: Finite Element Mesh

8. Model parameters

Thermal properties such as thermal conductivity, specific heat, density, and latent heat of vaporization are obtained from Polley et al., (1980) and Sanz et al., (1987) and used in the modeling. The effect of latent heat of vaporization will be considered only during heating and not during holding or cooling. Specific heat of steam was used as the specific heat of food at temperatures greater than 106°C. The surface heat transfer coefficient was calculated by (Toledo, 1991).

$$h_t = 1.3196 \left(\frac{[T_s - T_a]}{D} \right)^{0.25} \quad (27)$$

The surface mass transfer coefficient is given by (Serenio and Medeiros, 1990)

$$\frac{h_t}{h_m \lambda_v} = 64.7 P_a / K \quad (28)$$

The penetration depth is given by (Nelson et al., 1994),

$$\delta_p = \frac{\delta_0}{2\pi(2\varepsilon')^{0.5}} \left[\left(1 + \left(\frac{\varepsilon''}{\varepsilon'} \right)^2 \right)^{0.5} - 1 \right]^{-0.5} \quad (29)$$

The dielectric properties ε' and ε'' were calculated for ground beef patties using predictive equations given by Gunasekaran et al., (2002a)

$$\varepsilon' = 50.69 - 0.08T + 0.0005T^2 - 1.23F + 0.03F^2 \quad (30)$$

$$\varepsilon'' = 16.70 - 0.05T + 0.0007T^2 + 0.22F \quad (31)$$

For frozen broccoli, ε' and ε'' were calculated using equations given in Gunasekaran et al., (2002b). The average of coefficients for florets and stem parts were used to obtain coefficients for ε' and ε'' ,

$$\varepsilon' = 73.55 - 0.25T + 0.001T^2 \quad (32)$$

$$\varepsilon'' = 18.85 - 0.165T + 0.00145T^2 \quad (33)$$

The saturated vapour pressure of air with respect to temperature is given by Weiss (1977):

$$P_s = 614.97 \exp \left[17.2694 \left(\frac{T - 273}{T - 35.7} \right) \right] \quad (34)$$

Partial vapour pressure will be calculated by multiplying the saturated vapour pressure by relative humidity of air or by water activity of food.

9. Simulation results and discussions

The cavity is excited by one magnetron (frequency 2.45 GHz, average power 1 kW) through the waveguide feeder where the dominant (TE_{10}) mode is generated; the walls are of perfect electric conductivity. The electric field in the oven simulated by EMC2000-VF and visualized by HyperMesh is shown in Figure 8a.

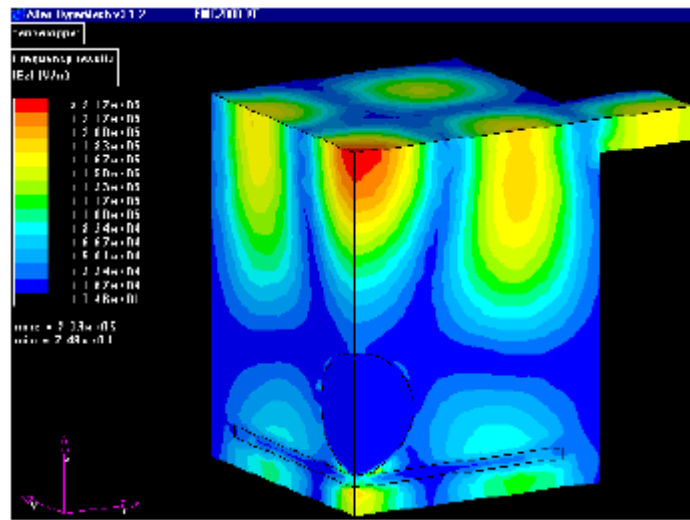


Fig 8a

In Figure 8b is shown SAR in the horizontal cut (QuickWave-3D)

The structure turns out to be highly resonant; at the operating frequency, the level of reflections is equal to -6.6 dB, i.e., about 22% of energy is reflected back to the magnetron. The patterns of dissipated power suggest that the food sample is very non-uniformly heated.

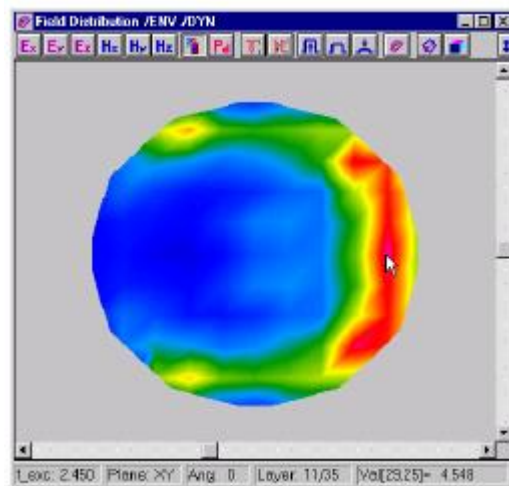


Fig 8b

The patterns of dissipated power within a food sample in a thin-wall package placed in a MW oven have been also obtained with the use of QuickWave-3D. The scenario designed for the Daewoo 800 W domestic oven (internal size 320 x 330 x 214 mm) includes the cylindrical product placed in the rectangular paper box consisting of two equivalent bottom and top parts with 1mm gap between them.

The box is centered on the bottom of the oven (Figure 9). The QuickWave's model has been built on the basis of this scenario. Computation was performed on the mesh of the cubic cells of 4 x 4 x 4 mm size; the total number of the cells in the model was about 570,000.

The Figure 9 shows the computed heat release within the absorbing materials, i.e., the packaging box and the food sample. It includes the SAR patterns in the three 6mm horizontal layers. It is seen that the chosen product in the given oven will be heated extremely nonuniformly.

Each cross-section possesses a significant “hot spot” placed between the center and the left surface of the cylinder facing the open end of the exciting waveguide. The maximum value of dissipated energy in these areas varies with the height and appears to be largest at the level about $\frac{1}{4}$ of the height of the sample from the bottom. The only cross-section with relatively uniform energy distribution (the top of the cylinder, the max/min ratio in the pattern is about 3.5) is associated with the smallest value of the dissipated power.

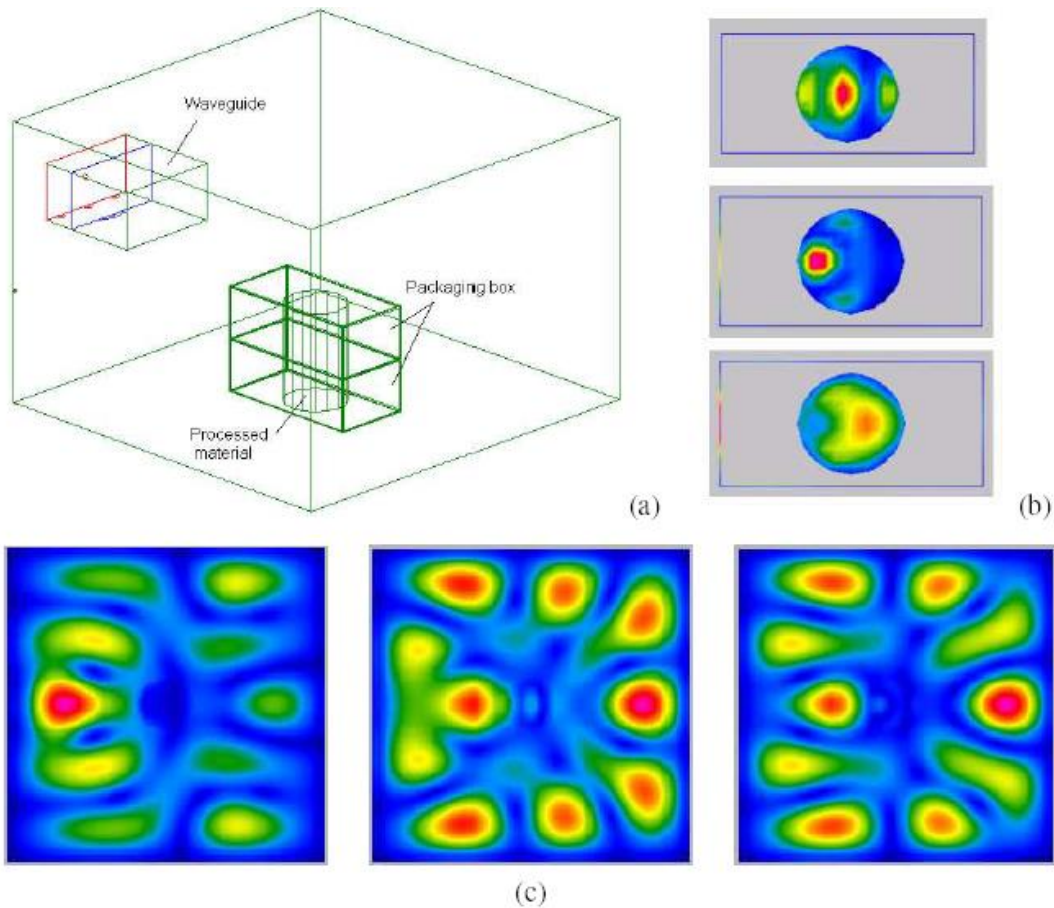


Figure 9. A standard 2.45 GHz oven with the cylindrical food sample (diameter 50 mm, height 74 mm, $\epsilon = 10.6 - i3.5$, conductivity $\sigma = 0.47$ S/m, density $\delta = 0.48$ g/cm³) in the paper box (120 x 60 x 80 mm, thickness 1 mm, $\epsilon = 2.6 - i0.9$, $\sigma = 0.122$ S/m, $\delta = 1.2$ g/cm³) (a): SAR patterns in the sample's top (72.5 mm from the oven's bottom), center (38 mm), and bottom (3.5 mm) horizontal 6 mm layers (b); dominating (vertical) component of the electric field in the horizontal cuts at the same heights respectively (c).

It turns out that the bottom wall of the package is strongly overheated. In the “hot spot”, the value of dissipated energy is even larger than the maximal energy released

in the processed material. This happens in spite of the fact that the sample product is characterized by larger values of complex permittivity than the box material and the thickness of the package wall is only 1 mm. The long vertical walls encounter insignificant heating.

The central parts of the short walls are overheated with the ratios about 100 and 30 for the wall in front of the waveguide and for the opposite one respectively. The maximum values of energy released in these box walls are comparable with the maximal values of energy in the “hot spots” of many cross-sections of the food sample.

Computational experiment conducted for the same cavity and the load but in the absence of the package box shows practically no difference in the SAR patterns of the food sample. This observation suggests that packages made from typical paper-based materials can sustain overheating even if the thickness of the walls is very small. However, such packages are unable to really change the heat pattern of the processed product contained within. This point resulted from the computer simulation appears to be consistent with the reasoning derived from the analytical approach estimated characteristics of the efficient controlling materials.

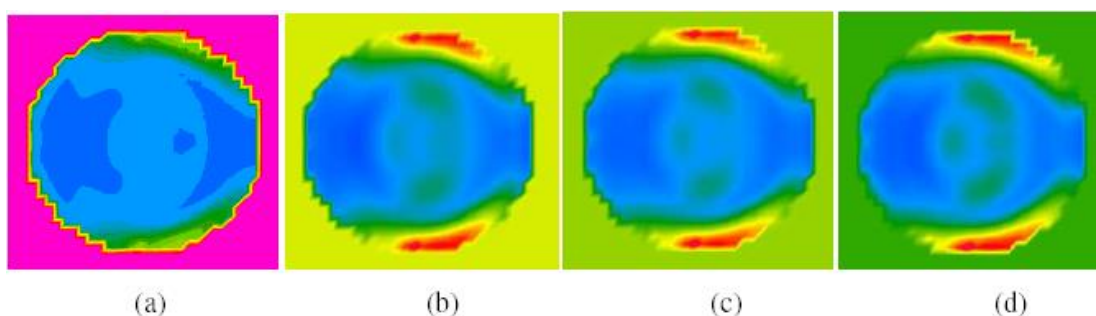


Figure 10 Temperature distributions in the top horizontal 2 mm layer of the 1-liter water cylinder in 1 (a), 2 (b), 3 (c), and 6 (d) minutes starting from the initial temperature of $T = 5^{\circ}\text{C}$ constant throughout the layer. Max/min values of temperature in the patterns are 18/6, 28/7, 34/8, and 40/10 $^{\circ}\text{C}$ respectively.

In Figure 10 is shown the analysis of the temperature patterns suggests that heating of the top layer of 1 liter of water load is characterized by strong “hot spots” along the cylinder’s edges. Air around the load possesses constant temperature (20 $^{\circ}\text{C}$), but since the patterns reproduce the relative temperature distributions, the air area appears in different colours from purple (a) through yellow (b) to green (d)). The rate of heating of the water cylinder is slightly decreased, but (at least within the present time interval) the trend of the pattern is not changed.

10. The rotating turntable

Once the microwaves have been coupled into the cooking chamber, they are effectively reflected by the metallic walls. The waves resonate in the cavity and form standing waves. The analysis of these standing waves is simplified by the fact that the

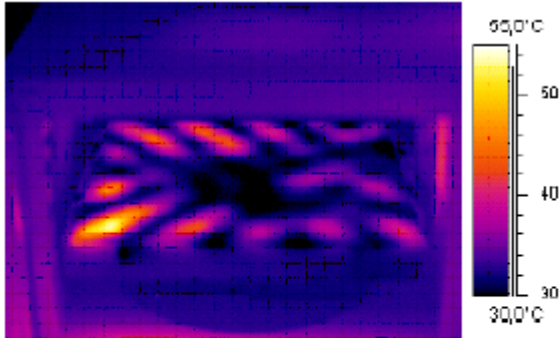


Figure 11 Visualization of the horizontal mode structure in a microwave oven using infrared thermal imaging. A glass plate with a thin water film was placed at a height of 8 cm and heated for 15 s with a microwave power of 800 W without using the turntable

wavelength of the microwaves is roughly the same as the linear dimensions of the chamber.

An ideal microwave oven cooks all food evenly but the nodes and antinodes of the standing waves can cause the food to burn in some places but to remain cool in others. The homogeneity of the field distribution may be estimated theoretically from the number of modes that may be excited within a narrow frequency range

close to the magnetron frequency (see below) or studied experimentally. Figure 11 shows the intensity distribution within an oven of 29 X 29 X 19 cm³ at height of about 8 cm.

A horizontal glass plate covered with a thin film of water was placed in a microwave (without its rotating turntable) on full power (800 W) for about 15 s. The false colour image was obtained with a thermal infrared camera. With only a small amount of water present, the image shows the microwave intensity distribution in a nearly empty chamber. There is a pronounced horizontal mode structure, which would lead to uneven heating of food.

This is the reason for having a rotating turntable: the rotation will move the food in and out of the hot spots. Some ovens have a mode stirrer, i.e. a rotating reflector at the top to get a more homogeneous field distribution, and there are investigations into how geometrical changes of the wall structure may improve the situation.

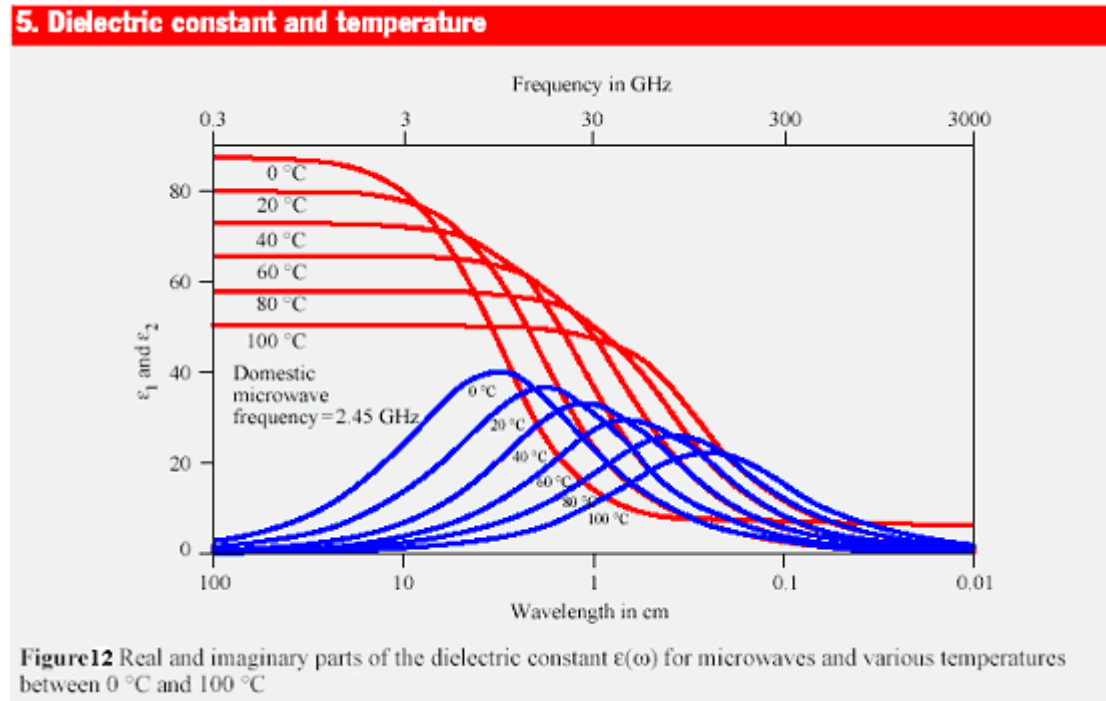
11. The average microwave power

Quantitatively, the average microwave power absorbed by a dielectric may be written as:

$$P = \omega \epsilon_0 \epsilon_2 E_{eff}^2 V \quad (35)$$

where V is the volume of the dielectric and E_{eff} the square of the average electric field within this volume. ϵ_0 is the imaginary part of the dielectric constant $\epsilon = \epsilon_1 + i\epsilon_2$. For pure liquid water, the changes of $\epsilon_1(\omega)$ and $\epsilon_2(\omega)$ are displayed schematically in figure 12 for various temperatures. These curves are considered to be typical for most kinds of food containing water.

Since food is usually heated from about room temperature to, say, 100 °C, figure 12 suggests that choosing a frequency between 10 and 100 GHz will produce optimum power absorption according to equation (35). As a matter of fact, a different physical criterion decides which frequency to choose.



12. Penetration depths of microwave in water

Using $\epsilon = n_2$ one may calculate the imaginary part of the refractive index and from this the absorption coefficient α , which is related to the penetration depth δ of the electromagnetic waves (equation $\delta = \lambda/4 \cdot \pi \cdot n_2$) by $\alpha = 1/\delta$. Figure 13 gives a crude overview in the form of a double logarithmic plot of the absorption coefficient of water from the microwave region (0.1 GHz) to the UV region (10^{16} Hz). Obviously water shows a very pronounced increase of the absorption coefficient with frequencies extending into the IR region. This may even lead to $\alpha > 10^3 \text{ cm}^{-1}$, which corresponds to penetration depths δ of less than 10 μm . Between the vibrational excitations in the IR and the electronic excitations

in the UV, there is the well known minimum of $\alpha \leq 10^3 \text{ cm}^{-1}$ in the visible, which leads to δ well above 10 m for clear water, i.e. the high transmission of water experienced every day.

Figure 13 also explains why microwave ovens use a frequency of about 2.45 GHz rather than 20 to 1000 GHz, as may have been guessed from Figure 13. With increasing frequency, α increases rapidly, i.e. the penetration depth $\delta = 1/\alpha$ decreases rapidly. The food

in microwave ovens has typical dimensions of the order of cm, and hence the penetration depth should be in this range. With a frequency of 20 GHz, the penetration depth would be much smaller, i.e. the energy would be absorbed in a thin surface layer of the food (toasting the food) while the interior would remain cold. The lower frequency chosen results in absorption of the microwaves everywhere in the food. Therefore the surface will only get a brown crust if additional grilling facilities are available.

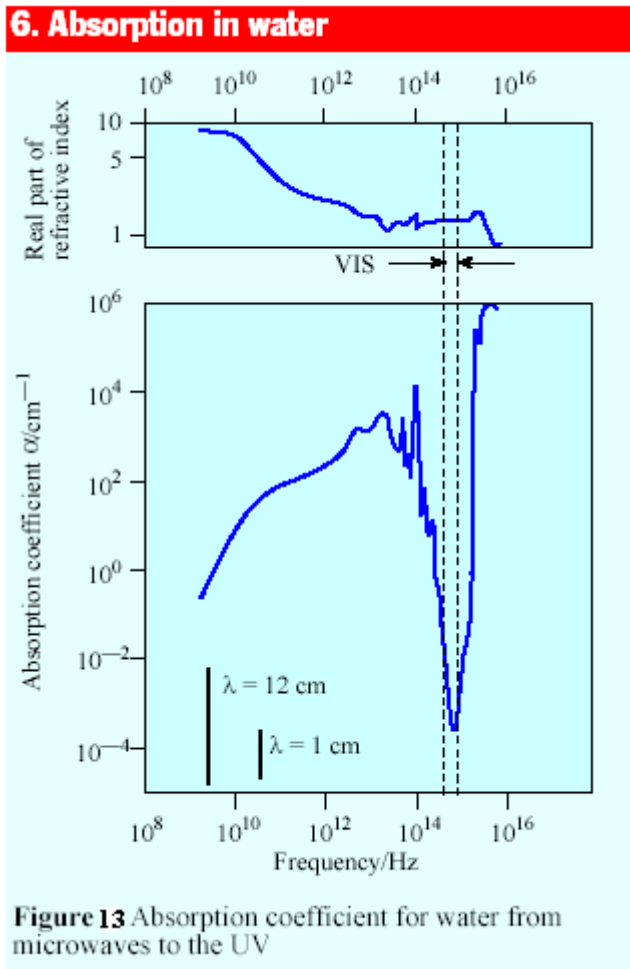


Figure 13 Absorption coefficient for water from microwaves to the UV

13. Conclusions

By analysing the results obtained by the program that computed the resonance frequency, it can be seen that in the first stage, when we had the air as dielectric, for the initial sizes we did not obtain the desirable resonance frequency in any of the studied propagation mode, so that is necessary to modify one of the dimensions of the applicator in order to obtain the resonance frequency $f = 2.45 \text{ GHz}$.

References

1. A. Breccia, A. Fini, A. Feroci, G. Grassi, B. Dellonte, S. Mongiorgi
Coupled Systems Dielectric microwave to improve Thermal Effects. J Microwave Power and Elm. 30,1,1995
2. F. Gardiol
Hyperfrequencies Ed. Georgi, Lausanne, 1981
3. W. J. L. Jansen, B. J. C. Wekken
Modelling of Dielectrically Assisted Drying J.Microwave Power and Elm. Energy vol 26,p. 119, 1991
4. C. W. Townbridge
Computing Electromagnetic Fields for Research and Industry, major achievements. and future trends, IEEE Trans on Mag.,32(3),1996
5. Peter A. Rizzi
Microwave engineering passive circuits, Prentice Hall, 1st edition (December 1, 1987)
6. Clayton R. Paul, Keith W. Whites, Syed A. Nasar
Introduction to Electromagnetic Fields, The McGraw-Hill, McGraw-Hill College, 3rd edition (December 9, 1997)
7. Paul Reitz, Frederick J. Milford, Robert W. Christy
Foundations of Electromagnetic Theory, Addison Wesley; 4th edition (October 31, 1992)
8. S.R. Pennock, P.R. Shepherd
Microwave Engineering with wireless applications, McGraw-Hill Professional Publishing (May 1, 1998)
9. A. Kokkosis
Determining the sensibility of the power magnetron with the WTh cathode with direct heating, depending on the accuracy of execution of the anode and cathode
4th International Conference on Renewable Sources and Environmental Electro -Technologies, June 6 – 8, 2002, Stana de Vale – Spa – Romania, pp. 152 – 157, 2002.
10. David M. Pozar
Microwave Engineering, Wiley; 3 edition (February 5, 2004)
- 11.C. Kokkonis, A. Kokkosis
Microwave Heating Electromagnetic Field Profiles, Scientific Review of Applied Research of TEI Piraeus, Volume XII, No 1, 2007 pp.39-47.
- 12.M. Tomse S. Pasca A. Kokkosis
Comparison Between Results of Numerical Simulation of Electromagnetic Forming Applied on Metallic Workpieces Using Different Software, 7th International Conference on Renewable Sources and Environmental Electro-Technologies, RSEE 2008, 29-30 May 2008, Oradea Romania, pp. 144 – 148, 2008.

